Physical model for the exotic ultraviolet photo-conductivity of ZnO nanowire films*

Pan Yue-Wu(潘跃武)[a], Ren Shou-Tian(任守田)[b], Qu Shi-Liang(曲士良)[b], and Wang Qiang(王 强)[b]†

[a] *Mathematics and Physical Sciences Technology, Xuzhou Institute of Technology, Xuzhou* 221008, *China*
[b] *Department of Optoelectronic Science, Harbin Institute of Technology at Weihai, Weihai* 264209, *China*

(Received 18 May 2013; revised manuscript received 8 July 2013)

Employing a simple and efficient method of electro-chemical anodization, ZnO nanowire films are fabricated on Zn foil, and an ultraviolet (UV) sensor prototype is formed for investigating the electronic transport through back-to-back double junctions. The UV (365 nm) responses of surface-contacted ZnO film are provided by *I*–*V* measurement, along with the current evolution process by on/off of UV illumination. In this paper, the back-to-back metal–seconductor–metal (M–S–M) model is used to explain the electronic transport of a ZnO nanowire film based structure. A thermionic-field electron emission mechanism is employed to fit and explain the as-observed UV sensitive electronic transport properties of ZnO film with surface-modulation by oxygen and water molecular coverage.

Keywords: ZnO nanowires, metal–semiconductor–metal contact, water modulated surface barrier, thermionic-field electron emission

PACS: 81.16.Be, 81.07.Gf, 72.10.–d **DOI:** 10.1088/1674-1056/22/11/118102

1. Introduction

Low-dimensional materials and physics have drawn intensive attention in recent years. One-dimensional (1D) semiconductor nanomaterials have been especially of concern because of their promising applications in nanoscale electronic and optoelectronic devices, such as field effect transistors,[1,2] gas and chemical sensors,[3,4] and photodetectors.[5,6] However, the metal/semiconductor contact (Ohomic or Schottky contact) emerges as a pivotal problem for the performances of above-mentioned electronic devices, owing to the much exacerbated accumulating of surface states for a nanomaterial.[7–9] An Ohmic contact is obligatory for the fabrication of some phtoto-sensors (e.g. silicon sensors), while a Schottky contact is particularly required to form light and gas sensors with high and quick response for metal oxide nanomaterials such as ZnO and TiO_2.[10,11] As far as we know, the sensitivity and stability of ultraviolet (UV) sensors based on metal oxide nanomaterials still need to be further improved, and the study of sensing mechanisms is therefore rather urgently needed. However, there is a scarcity in this research trend.

As reported previously,[7,12,13] the underlying UV sensing mechanism of metal oxides is that the surface states of nanostructured metal oxides can be greatly modulated by adsorbed oxygen and water species, and the density of surface trapped electric charges can be efficiently and reversibly modified by photo exposure, introducing large and reversibly quick modulation of surface barrier. As is well known, studies have seldom been conducted to systematically figure out the relation between surface state evolutions of nanostructured metal oxides using UV light, hence the corresponding work is urgently required to guide the fabrication of high performance UV sensors.

In this paper, ZnO nanowire films are fabricated on Zn foil by following a typical electro-chemical method, and a high-sensitivity UV sensor prototype is formed. The thermionic-field electron emission mechanism is used to fit and explain the as-observed UV sensitive properties of ZnO film with a surface coverage of water molecular and oxygen species. As should be noted, the thermionic-field electron emission mechanism is a compromised theory between the thermionic emission model and the barrier-tunneling model, which is an effective formalism for treating complicated electronic transport processes through a metal–semiconductor barrier.

2. Experiment

ZnO nanowire film was grown on Zinc foil by following a standard anodization process in a home-made electrochemical cell. Zinc foil (99.999% purity) with a thickness of 0.5 mm was used as an anode. The single-side surface area of the anode was 2×3 cm^2. The cathode was a graphite plate with an area of 2×4 cm^2, which was placed just below the zinc foil with an inter-electrode distance of 10 cm. The liquid/air interface region of the Zinc foil was protected by resin coating, which is critical for preventing the interface-reaction therein and thus converging the etching current between par-

*Project supported by the National Natural Science Foundation of China (Grant Nos. 11274082 and 51172194) and the Excellent Young Scientist Research Award Fund of Shandong Province, China (Grant No. BS2011CL002).

†Corresponding author. E-mail: wq750505@hotmail.com

© 2013 Chinese Physical Society and IOP Publishing Ltd

allel inter-electrode regions. As we see, it is important to form high-quality ZnO nanowires. Finally, final products with white color and shaggy morphology were obtained. Other experimental details are similar to those described in our previous paper.[14]

In the anodization process, both chemical and electrochemical processes were used to etch the zinc foil. At a high voltage of 10 V in our experiment, the electrochemical etching dominates the whole anodization process. Reactions took place during the anodization of Zn and can be represented as follows: at the cathode,

$$2H^+ + 2e^- \rightarrow H_2 \ \ (\text{gas}), \tag{1}$$

at the anode,

$$Zn - 2e^- \rightarrow Zn^{2+}, \tag{2}$$

$$Zn^{2+} + 2OH^- \rightarrow Zn(OH)_2 \ \ (\text{solid}), \tag{3}$$

$$Zn(OH)_2 + 2OH^- \rightarrow Zn(OH)_4^{-2}. \tag{4}$$

At the initial stage, $Zn(OH)_4^{-2}$ was formed and the surface of the zinc foil became uneven due to both chemical and electrochemical etching. The uneven zinc surface leads to the non-uniform electric field distribution and formation of dense "hot spots", which have a greater opportunity to absorb the negatively charged $Zn(OH)_4^{-2}$. In the anodization process, that negatively charged $Zn(OH)_4^{-2}$ products congregated at the "hot spots" on the surface of zinc foil, and formed nanowires. After annealing in air, zinc hydroxide on the surface of the foil decomposed into crystalline nanopraticles arranged in a line-like structure to form the as-observed ZnO nanowire.

Field emission scanning electron microscope (FE-SEM) and transmission electron microscopy (TEM) were used to characterize the surface morphologies and structural features of the nano-structured ZnO film. Photoluminescence (PL) and Raman spectra were used to investigate the optical and crystallographic properties of the ZnO film. A standard electrical measurement setup was used to obtain current–voltage (I–V) curves and current evolution spectra at UV illumination. UV photo-response measurements were obtained with a 6-W xenon arc lamp light source (365 nm). A variant humidity source was obtained by employing several saturated salt solutions as described in our previous paper.[15]

3. Results and discussion

3.1. Morphological characterization

After anodization and annealing, the anodized zinc foil was covered with a layer of white product. The morphology of the product was examined by using an FE-SEM and a TEM. The SEM image of the as-synthesized ZnO is given in Fig. 1(a), which reveals a large quantity of nanowires with uniform diameter. The lengths of the nanowires are tens of microns, and can be controlled by varying the reaction time. The detailed structures of ZnO nanowires were characterized using a TEM. Figure 1(b) shows a typical TEM image of the ZnO nanowires. The diameter of single nanowire is about 150 nm. The nanowire is covered with many nano-crevices, which increase the effective surface area for oxygen and water adsorption. A sponge-like structure is observed in Fig. 1(b), indicating that the ZnO nanowire is actually composed of nanocrystals. The sponge-like structure may be the plausible key reason for the high oxygen and water adsorption ability in the following discussion.

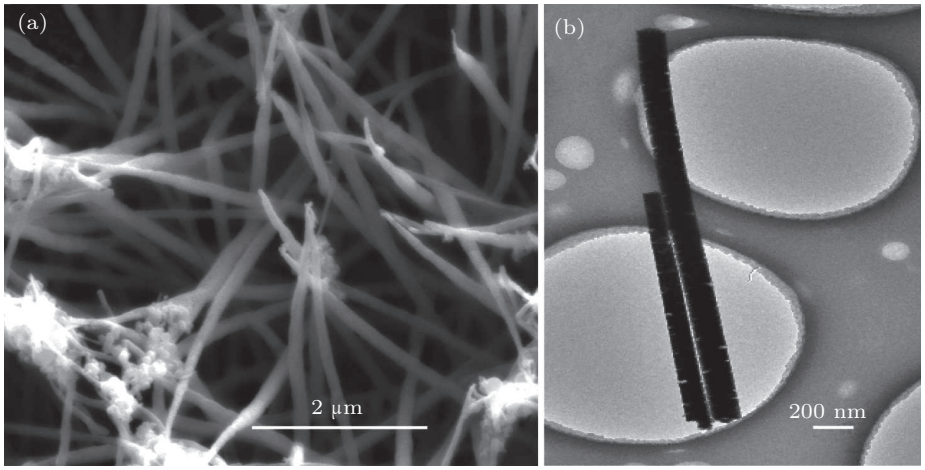


Fig. 1. Morphologies of the as-anodized zinc foils. (a) SEM image of the ZnO nanowires. (b) TEM image of the ZnO nanowire.

4. Photoluminescence and Raman spectra

The PL spectrum of the synthesized ZnO is shown in Fig. 2(a). Compositions of Gaussian line shapes are used to fit the PL spectrum for the peak position. Three peaks are identified at 386 nm (ultraviolet band), 556 nm (green band), and 629 nm (orange band). The UV near-band emission is usu-

ally described as the direct inter-band recombination of photo-generated charge carriers. The green emission (556 nm) is associated with emissions from deep levels caused by the structural defects such as oxygen vacancies, interstitial oxygen, and interstitial oxygen generated in the anodization process.[16] The orange emission (629 nm) arises from optical transitions in the single negatively charged interstitial oxygen ions (O_i^-) inside the grain. O_i^- is formed when some oxygen ions enter into the interstitial sites of the ZnO crystal lattice. The orange emission is attributed to the radiative recombination of a delocalized electron to the conduction band with a deeply trapped hole in O_i^- centers.[17] The above results indicate the existence of oxygen-related defects, which is favorable for the following explanation of the oxygen-related UV response of ZnO nanowires.

Figure 2(b) shows the Raman spectrum of ZnO nanowire film at room temperature. A sharp peak at 438. 8 cm^{-1} is observed, which is the characteristic band of the Raman-active E_2 mode of wurtzite hexagonal ZnO. Four weak peaks at 333.5, 380.8, 584.3, and 661.4 cm^{-1} corresponding to the $2E_2$, A_1(TO), E_1(LO), and A_1 vibration modes respectively, are observed in the low wave-number region. In the large wave-number region from 1000 to 1350 cm^{-1}, a strong peak at 1096 cm^{-1} is observed, corresponding to $A_1 + E_2$ mode. The existence of the E_1(LO) mode is associated with lattice defects, such as oxygen vacancy and zinc interstitial.[18] Lattice defects are confirmed by PL and Raman spectra. It should be mentioned that lattice defects make ZnO film more effective to adsorb oxygen and water molecules.

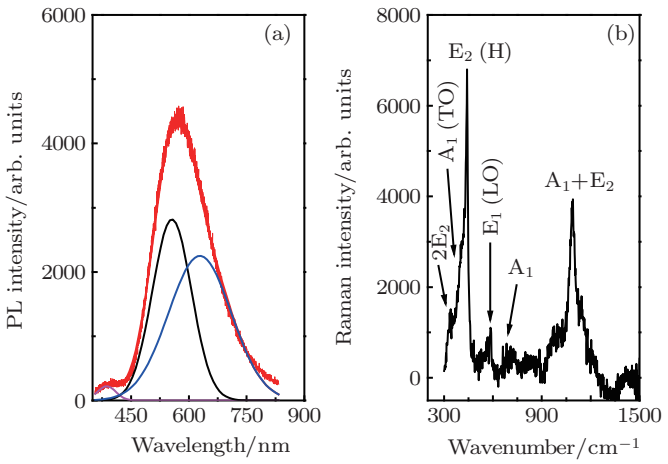


Fig. 2. (color online) (a) PL and (b) Raman spectra of zinc foil anodized at 10 V for 4 h, followed by annealing at 250 °C for 60 min in air.

4.1. UV sensitive electronic transport properties of the ZnO M–S–M structure

Current–voltage (*I–V*) characteristics of the ZnO nanowire films in the dark and upon UV illumination are shown in Fig. 3. A schematic of the circuit used for measuring UV and humidity responses is illustrated in the inset of Fig. 3(a). *I–V* plots of the ZnO film are neither linear nor rectifying, instead they have a little asymmetrical nonlinear behavior, indicating the existence of asymmetrical barriers between the ZnO film and Cu leads. It is noticeable that the current is greatly enhanced by UV illumination.

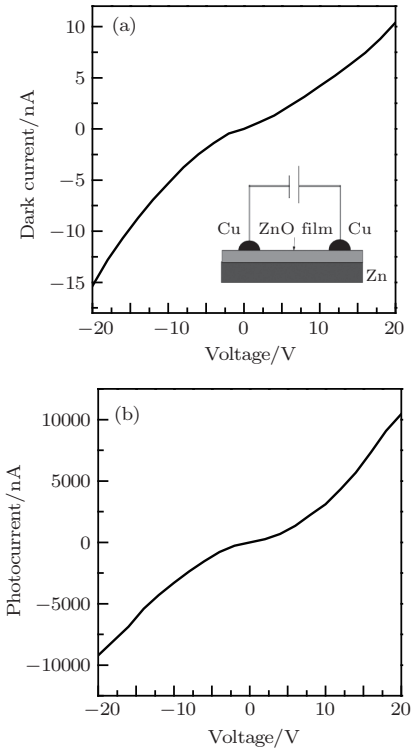


Fig. 3. *I–V* plots of ZnO film measured (a) in dark and (b) under UV illumination.

According to the work of Peng *et al.*[17] and Liao *et al.*,[18,19] especially our previous work on the electronic transport of individual graphitic fiber,[20] a back-to-back double diode model can be employed to explain the electronic transport properties of ZnO nanowire film modulated by humidity and ultraviolet illumination. The schematic diagrams of the back-to-back double diodes model and relevant energy band are shown in Fig. 4.

Figure 4(a) is the schematic diagram of back-to-back double metal–semiconductor (MS) junctions of ZnO nanowires film. Figures 4(b) and 4(c) illustrate the energy band diagrams of the junctions for zero, positive bias, respectively. It will be clarified subsequently that ZnO semi-conducting film behaves as a normal resistor with constant resistance, as long as the contact effect and electrical heating effect are neglected. The nonlinear *I–V* plot is the manifestation that MS junctions dominate electronic transport in this system, especially for the reversely biased junction. Owing to the high density of surface states via the absorption of oxygen molecules on the ZnO

surface, an insulating surface layer (carrier depletion layer) is formed, resulting in the up-bending of energy band structure, as shown in Figs. 4(b) and 4(c). For MS contacting, a unique effect is introduced: the contact barrier Φ_b is insensitive to the work function of metal, and can merely be determined by the surface up-bending potential $\Phi_{surface}$, in direct relation with semiconductor surface adsorption states. In Fig. 4, the bias V_{bias} applied between Cu wire and Cu wire must be assigned as

$$V_{bias} = V_1 + V_2 + V_3, \tag{5}$$

where V_1 is the voltage drop on Cu–ZnO MS barrier (barrier 1), V_2 is the voltage drop on the film body, and V_3 is the voltage drop on the MS barrier (barrier 2). V_1, V_2, and V_3 are combined to construct the total applied voltage V, while their dependences on total applied voltage V are nonlinear. This non-linearity is the characteristic of a back-to-back M-SM structure, which is composed of different parts, thermionic-field emission, ohmic transport and thermionic emission for reverse-bias junction, ZnO body and positive-bias junction, respectively, with different electrical transport mechanisms.

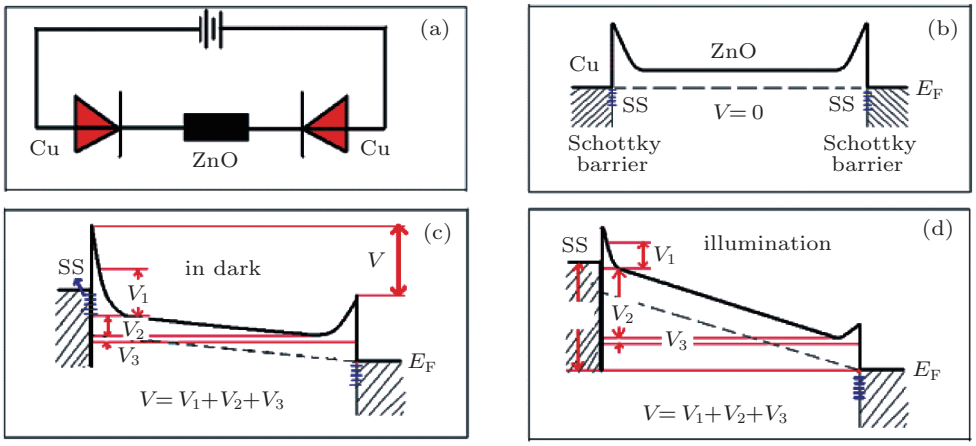


Fig. 4. (color online) Schematic diagram of back-to-back double diode model (a). Energy band diagrams of the metal-ZnO-metal structure without bias (b), under bias V (c), under bias and UV illumination(d). SS denotes the surface states.

As shown in Fig. 4(c), at positive bias, the barrier 2 on the ZnO side is lowered to permit efficient thermionic electron conduction with comparatively low resistance, and no electron tunneling. The voltage assigned to the positively biased junction is negligible. The transport current can then be expressed as

$$I = I_{sat2}\left[\exp\left(\frac{qV_3}{kT}\right)\right], \tag{6}$$

where I_{sat2}, q, k, and T are the saturation thermionic current of barrier 2, the elementary charge, Boltzmann's constant, and the temperature, respectively.

Barrier 1 can be modeled as a reversely biased MS junction, and only a rather low saturation current should be detected in the ideal case. However, considering the ever-raising current versus applied voltage in our I–V plots in Fig. 3, thermionic-field emission (TFE) of majority carriers through the reversely biased MS junction is proposed as the explanation for the electric current at high applied biases. Thermionic-field emission current through the reversely biased MS junction can be expressed as[21]

$$I_{TFE} = AJ_S \exp\left(\frac{q(V_1+V_p)}{\varepsilon'}\right), \tag{7}$$

where

$$J_s = \frac{A^*T(\pi qE_{00})^{1/2}}{k}\exp\left(-\frac{q(\phi_B - V_p)}{E_0}\right) \times \left[V_1 - V_p + \frac{\phi_B}{\cosh^2(E_{00}/kT)}\right]^{1/2}, \tag{8}$$

$$\varepsilon' = \frac{E_{00}}{E_{00}/kT - \tanh(E_{00}/kT)}, \tag{9}$$

where A is the effective contact area at the reverse-Schottky barrier, ϕ_B is the effective barrier height of the reverse-Schottky barrier height, V_1 is the voltage drop on the reverse-Schottky barrier, A^* is the Richardson constant, k is Boltzmann's constant, T is the absolute temperature (300 K), J_s is the saturation current density, ε' is a non-dimensional parameter, and the parameters are given as $V_p = 0.1$ eV, $A^* = 38.2$ A·cm^{-2}·K^{-2}, $E_0 = 26.2$ meV, and $E_{00} = 3.52$ meV.[17]

When $V_1 \gg \phi_B$, the current dependence on junction bias V_1 can be reduced to

$$I_{TFE} = CV_1^{1/2}\exp\left(\frac{q(V_1+V_p)}{\varepsilon'}\right), \tag{10}$$

$$C = \frac{AA^*T(\pi qE_{00})^{1/2}}{k}\exp\left(-\frac{q(\phi_B - V_p)}{E_0}\right). \tag{11}$$

Thus, we can deduce that

$$\ln\frac{I_{\rm TFE}}{V^{1/2}} \propto V_1. \tag{12}$$

For the current through the ZnO film, it certainly follows the Ohmic law: $I = V_2/R_{\rm ZnO}$.

Since the current through the three devices connected in series should be equal, another restriction among the three biases is obtained as

$$\begin{aligned} I &= AJ_{\rm S}\exp\left(\frac{q(V_1+V_{\rm p})}{\varepsilon'}\right) \\ &= I_{\rm sat2}\left[\exp\left(\frac{qV_3}{kT}\right)\right] = \frac{V_2}{R_{\rm ZnO}}. \end{aligned} \tag{13}$$

Equation (12) shows that $\ln(I/V^{1/2})$ is proportional to the voltage drop V_1 on the reverse-Schottky barrier. As shown in Fig. 5, in the dark, $\ln(I/V^{1/2})$ is proportional to the bias V at large positive and negative bias from 11 to 20 V. Under UV illumination, $\ln(I/V^{1/2})$ becomes proportional to the bias V at large positive and negative bias (absolute value) of 8 V$<$V$<$ 14 V. As the positive or negative bias V (absolute value) exceeds 14 V, $\ln(I/V^{1/2})$ is no longer proportional to bias V, instead it shows somehow current saturated characteristics. We propose that the current saturation phenomenon is probably due to a large injection effect, while the exact explanation is still under study. Both $\ln(I/V^{1/2})$–V plots show derivations from linear properties at relatively low bias, which indicates that the derivation originates from the approximation condition $V_1 \gg \phi_{\rm B}$.

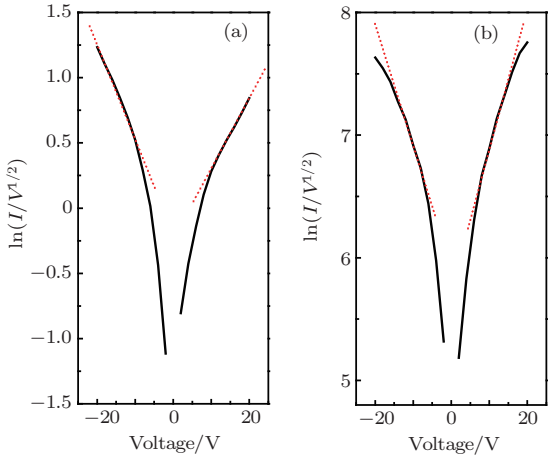


Fig. 5. (color online) $\ln(I/V^{1/2})$–V plots (a) in dark and (b) under UV illumination. The solid curves represent experimental results obtained from I–V plots in Fig. 3, and the dotted lines denote the fitted results.

The above results indicate that in the dark the bias V applied between the electrodes is dropped mostly on the large reverse-Schottky barrier, so $V_{\rm bias}$ is almost equal to V_1. When UV light is on, the Schottky barrier is efficiently lowered by the desorption of oxygen molecules as suggested in our previous paper.[14] As applied voltage V is increased, V_1 becomes progressively smaller than the bias V, because part of bias V is applied on ZnO film, which explains the saturation characteristics of $\ln(I/V^{1/2})$ at the higher bias V.

In UV photo-response characterization, photo-conductivity gain G is an important parameter. The full expression of photo-conductivity gain G, a non-dimensional parameter, as a function of applied voltage V, is modeled as

$$G(V) = \frac{N_{\rm e-p}}{N_{\rm ph}} = \frac{h\upsilon}{Pq}\Delta I(V) \propto \Delta I(V), \tag{14}$$

where $N_{\rm e-p}$ is the number of electrons collected per unit time, $N_{\rm ph}$ is the number of absorbed photons per unit time, P is the incident UV light power at the sensing area, q is the elementary charge, ν is the incident light frequency, and $\Delta I(V)$ is the difference between photo-current and dark current. The sensing area is difficult to determine, so the incident UV light power is unknown. Quantitative gain $G(V)$ cannot be obtained. The linear relationship between $G(V)$ and $I(V)$, ΔI–V relation can be used to explain the $G(V)$–V relation.

ΔI–V relation is illustrated in Fig. 6. At sufficiently high voltage above 14 V, ΔI (also G) shows linear dependence on applied voltage, indicating e–p generation and transport in ZnO dominate the UV response process, which is in good consistence with the discussion above. The linear ΔI–V relation illustrates the intrinsic photo-response of ZnO UV detector, and well follows the standard rule:[22]

$$G(V) \approx \frac{1}{L^2}\eta\tau\mu V \propto V. \tag{15}$$

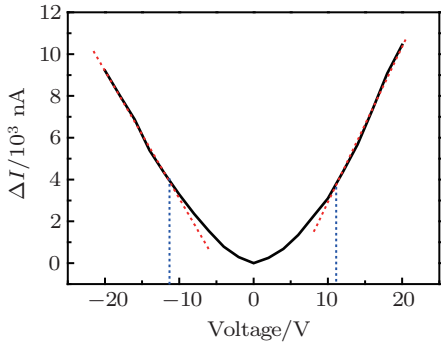


Fig. 6. (color online) ΔI–V relation obtained from I–V plots in the dark and under UV illumination.

At lower voltage, the nonlinear ΔI–V relation deviates from the standard rule, which can be certainly ascribed to the disturbance of voltage drop on the reverse M-S junction. At lower bias V, photo-current increases slowly as bias V increases. Thus, an essential conclusion is drawn: the existence of an M–S junction is detrimental to obtaining a high transport current, but the lowering of the M–S junction by desorption of O_2 species can enhance the photo-response. The detailed UV photoresponse of ZnO nanowire film at different bias voltages was studied in our previous work.[14] The combined effect of surface potential lowering from O_2^- species desorption

and conductivity enhancement from electron–hole generation is employed to explain the as-observed UV photoresponse of ZnO nanowire film, which is also applicable for our present study. The interaction between H_2O and ZnO is a complex process. There is currently no other experimental report on such a study. However, our study in this paper is similar to Nowotny *et al*.'s result on the interaction between H_2O and TiO_2 to explain the photocatalysis process.[23]

5. Conclusion

In this paper, ZnO nanowire films are fabricated by using a simple electro-chemical anodization method. The UV photoresponses of surface-contacted ZnO film are characterized using *I*–*V* plots and the current evolution process by turning UV illumination on/off. A back-to-back double diode model is employed to explain the as-observed UV sensitive electronic transport properties. The thermionic-field electron emission mechanism is employed to fit and explain the as-observed UV sensitive electronic transport properties. As the applied bias V increases, photo-conductivity gain is increased, which follows the typical characteristics of an M–S junction dominated photo-detector. Surface O_2^- species desorption, along with the photo-catalytic hydrolysis of water molecules plays a key role in the as-observed UV response of ZnO films. Considering the simple experimental conditions, the anodizing method provides a simple but powerful way to fabricate low-cost UV detectors.

References

[1] Mubeen S and Moskovits M 2011 *Adv. Mater.* **23** 2306
[2] Fan Z, Wang D W, Chang P C, Tseng W Y and Lu J G 2004 *Appl. Phys. Lett.* **85** 5923
[3] Ramgir N S, Yang Y and Zacharias M 2010 *Small* **6** 1705
[4] Huang J X, Virji S, Weiller B H and Kaner R B 2003 *J. Am. Chem. Soc.* **125** 314
[5] Hu L F, Yan J, Liao M Y, Wu M and Fang X S 2011 *Small* **7** 1012
[6] Li Y B, Valle F D, Simonnet M, Yamada I and Delaunay J J 2009 *Nanotechnology* **20** 045501
[7] Cheng G, Wu X H, Liu B, Li B, Zhang X T and Du Z L 2011 *Appl. Phys. Lett.* **99** 203105
[8] Hu Y F, Zhou J, Yeh P H, Li Z, Wei T Y and Wang Z L 2010 *Adv. Mater.* **22** 3327
[9] Li C, Bando Y, Liao M Y, Koide Y and Golberg D 2010 *Appl. Phys. Lett.* **97** 161102
[10] Wang S J, Lu W J, Cheng G, Cheng K, Jiang X H and Du Z L 2009 *Appl. Phys. Lett.* **94** 263106
[11] Mor G K, Shankar K, Paulose M, Varghese O K and Grimes C A 2006 *Nano Lett.* **6** 215
[12] Huang J and Wan Q 2009 *Sensor* **9** 9903
[13] Pearton S J and Ren F 2013 *Nanomater. Nanotechnol.* **3** 1
[14] Ren S T, Wang Q, Zhao F and Qu S L 2012 *Chin. Phys. B* **21** 038104
[15] Wang Q, Pan Y Z, Huang S S, Ren S T, Li P and Li J J 2011 *Nanotechnology* **22** 025501
[16] Liu Y, Wang S, Zhang Z Y and Peng L M 2008 *Appl. Phys. Lett.* **92** 033102
[17] Zhang Z Y, Jin C H, Liang X L, Chen Q and Peng L M 2006 *Appl. Phys. Lett.* **88** 073102
[18] Liao Z M, Liu K J, Zhang J M, Xu J and Yu D P 2007 *Phys. Lett. A* **367** 207
[19] Liao Z M, Hou C, Zhou Y B, Xu J, Zhang J M and Yu D P 2009 *J. Chem. Phys.* **130** 084708
[20] Wang Q, Gao R X, Qu S L, Li J J and Gu C Z 2009 *Nanotechnology* **20** 145201
[21] Liao M Y, Wang X, Teraji T, Koizumi S and Koide Y 2010 *Phys. Rev. B* **81** 033304
[22] Fàbrega C, Hernández-Ramírez F, Prades J D, Jiménez-Díaz R, Andreu T and Morante J R 2010 *Nanotechnology* **21** 445703
[23] Nowotny M K, Sheppard L R, Bak T and Nowotny J 2008 *J. Phys. Chem. C* **112** 5275